Inorg. Chem. **2002**, *41*, 3929–3934

Synthesis, Crystal Structure, and Solid State NMR Spectroscopy of $NH_4[(V_2O_3)_2(4,4'\text{-bpy})_2(H_2PO_4)(PO_4)_2]\cdot 0.5H_2O$, a Mixed-Valence Vanadium(IV,V) Phosphate with a Pillared Layer Structure

Ling-I Hung,[†] Sue-Lein Wang,*[,†] Hsien-Ming Kao,*[,‡] and Kwang-Hwa Lii*[,‡,§]

Department of Chemistry, National Tsing Hua University, Hsinchu, Taiwan 320, Republic of China, Department of Chemistry, National Central University, Chungli, Taiwan 320, Republic of China, and Institute of Chemistry, Academia Sinica, Nankang, Taipei, Taiwan 115, Republic of China

Received December 14, 2001

A mixed-valence vanadium phosphate, $NH_4[(V_2O_3)_2(4,4'\text{-bpy})_2(H_2PO_4)(PO_4)_2]\cdot 0.5H_2O$, has been synthesized under hydrothermal conditions and structurally characterized by single-crystal X-ray diffraction. It crystallizes in the monoclinic space group *C*2/*c* (No. 15) with $a = 12.6354(8)$ Å, $b = 9.9786(6)$ Å, $c = 23.369(1)$ Å, $\beta = 92.713(1)°$, and $Z = 4$ with $R_1 = 0.0389$. The structure consists of dimers of edge-sharing vanadium(IV,V) octahedra that are connected by corner-sharing phosphate tetrahedra to form layers in the *ab*-plane, which are further linked through 4,4′-bipyridine pillars to generate a 3-D framework. Magnetic susceptibility confirms the valence of the vanadium atoms. The ^{31}P MAS NMR spectrum shows a resonance centered at 80 ppm with a shoulder at ca. 83 ppm in an intensity ratio close to 1:2, which correspond to two distinct P sites. The observed large downfield ^{31}P NMR shifts can be ascribed to magnetic exchange coupling involving phosphorus atoms. The unpaired electron spin density at the phosphorus nucleus was determined from variable-temperature ^{31}P NMR spectra. The ^{1}H MAS NMR spectrum was fitted to six components in accordance with the structure as determined from X-ray diffraction.

Introduction

The synthesis of open-framework metal phosphates has been a subject of intense research owing to their interesting structural chemistry and potential applications in catalysis.[1−3] A large number of these materials are synthesized in the presence of organic amines as structure-directing agents. Recently, many researchers have used a hybrid approach in which an organic ligand is combined with an inorganic one.[3,4] The combination of these two kinds of ligands adds complexity to the structures. As compared with inorganic ligands, the organic ligands have larger sizes and a wide variety of means of connection. An interesting variant of the metal phosphate is obtained by incorporating the oxalate unit in the materials. A large number of oxalatophosphates of Fe,[5−10] V,[11,12] Al,[13] Ga,[14−16] In,[17] and Mn[18] have been

* Authors to whom correspondence should be addressed. E-mail: liikh@cc.ncu.edu.tw (K.-H.L.); hmkao@cc.ncu.edu.tw (H.-M.K.); slwang@mx.nthu.edu.tw (S.-L.W.).
† National Tsing Hua University.
‡ National Central University.
§ Institute of Chemistry, Academia Sinica.

(1) Haushalter, R. C.; Mundi, L. A. *Chem. Mater.* **1992**, *4*, 31, and references therein.
(2) Lii, K.-H.; Huang, Y.-F.; Zima, V.; Huang, C.-Y.; Lin, H.-M.; Jiang, Y.-C.; Liao, F.-L.; Wang, S.-L. *Chem. Mater.* **1998**, *10*, 2599.
(3) Cheetham, A. K.; Ferey, G.; Loiseau, T. *Angew. Chem., Int. Ed.* **1999**, *38*, 3268, and references therein.
(4) Hagrman, P. J.; Hagrman, D.; Zubieta, J. *Angew. Chem., Int. Ed.* **1999**, *38*, 2638, and references therein.
(5) Lin, H.-M.; Lii, K.-H.; Jiang, Y.-C.; Wang, S.-L. *Chem. Mater.* **1999**, *11*, 519.
(6) Lethbridge, Z. A. D.; Lightfoot, P. *J. Solid State Chem.* **1999**, *143*, 58.
(7) Choudhury, A.; Natarajan, S.; Rao, C. N. R. *J. Solid State Chem.* **1999**, *146*, 538.
(8) Choudhury, A.; Natarajan, S. *J. Mater. Chem.* **1999**, *9*, 3113.
(9) Choudhury, A.; Natarajan, S.; Rao, C. N. R. *Chem.-A Eur. J.* **2000**, *6*, 1168.
(10) Chang, W.-J.; Lin, H.-M.; Lii, K.-H. *J. Solid State Chem.* **2001**, *157*, 233.
(11) Tsai, Y.-M.; Wang, S.-L.; Huang, C.-H.; Lii, K.-H. *Inorg. Chem.* **1999**, *38*, 4183.
(12) Do, J.; Bontchev, R. P.; Jacobson, A. J. *Chem. Mater.* **2001**, *13*, 2601.
(13) Lightfoot, P.; Lethbridge, Z. A. D.; Morris, R. E.; Wragg, D. S.; Wright, P. A.; Kvick, A.; Vaughan, G. B. M. *J. Solid State Chem.* **1999**, *143*, 74.
(14) Chen, C.-Y.; Chu, P. P.; Lii, K.-H. *Chem. Commun.* **1999**, 1473.
(15) Lii, K.-H.; Chen, C.-Y. *Inorg. Chem.* **2000**, *39*, 3374.
(16) Huang, L.-C.; Kao, H.-M.; Lii, K.-H. *Chem. Mater.* **2000**, *12*, 2411.
(17) Huang, Y.-F.; Lii, K.-H. *J. Chem. Soc., Dalton Trans.* **1998**, 4085.
(18) Lethbridge, Z. A. D.; Tiwary, S. K.; Harrison, A.; Lightfoot, P. *J. Chem. Soc., Dalton Trans.* **2001**, 1904.

10.1021/ic011277i CCC: $22.00
Published on Web 06/21/2002

reported during past few years. A study of the literature about transition metal supramolecular architectures shows that the most extensively studied bridging organic ligand is 4,4′-bipyridine (4,4′-bpy).[4] We therefore extended our search for open frameworks into the 4,4′-bpy-phosphate system and have synthesized several interesting compounds. For example, $[Ga_4(4,4'\text{-Hbpy})(PO_4)(H_{0.5}PO_4)_2(HPO_4)_2(H_2PO_4)_2(H_2O)_2]\cdot H_2O$ is unique in such a way that among the vast number of synthetic phosphates and naturally occurring phosphate minerals it is the first example in which four different types of monophosphate are present in the same structure.[19] $[Ni(4,4'\text{-bpy})_2(H_2PO_4)_2]\cdot C_4H_9OH\cdot H_2O$ exhibits a new type of interpenetration involving a 2-D square net and a rarely observed 3-D $CdSO_4$-type framework of the same chemical composition.[20] $[(VO_2)_2(4,4'\text{-bpy})_{0.5}(4,4'\text{-Hbpy})(PO_4)]\cdot H_2O$ has a layer structure with the monoprotonated 4,4′-Hbpy ligand being coordinated to the vanadium(V) atom as a pendent group.[21] Here, we report a new member in the family $NH_4[(V_2O_3)_2(4,4'\text{-bpy})_2(H_2PO_4)(PO_4)_2]\cdot 0.5H_2O$, **1**, which consists of layers of mixed-valence vanadium(IV,V) phosphate pillared through 4,4′-bpy ligands into a 3-D structure. It is the first mixed-valence compound in the 4,4′-bpy-phosphate system. The synthesis, crystal structure, magnetic susceptibility, and solid state NMR spectroscopy are reported.

Experimental Section

Synthesis and Initial Characterization. The hydrothermal reactions were carried out in Teflon-lined stainless steel Parr acid digestion bombs with an internal volume of 23 mL. All chemicals were purchased from Aldrich Chemicals. Arsenic acid was prepared from a reaction of As_2O_3 and H_2O_2. Reaction of V_2O_5 (1 mmol), 4,4′-bipyridine (3 mmol), H_3PO_4 (6 mmol), $NH_4OH_{(aq)}$ (0.3 mL, 28%), and H_2O (12 mL) at 160 °C for 3 days produced dark green crystalline cubes of **1** in a yield of 60% based on vanadium. The pH of the reaction mixture before hydrothermal reaction was 3.1. The dark green color is indicative of a mixed-valence compound. Powder X-ray diffraction pattern of the bulk product is in good agreement with the calculated pattern on the basis of the results from single-crystal X-ray diffraction. Elemental analysis results of the bulk product are consistent with the stoichiometry of **1**. Anal. Found: C, 26.11; H, 2.49; N, 7.55. Calcd: C, 25.94; H, 2.50; N, 7.56. Attempts to synthesize the arsenate analogue under reaction conditions similar to those for **1** were unsuccessful. A vanadyl arsenate with a 1-D chain structure and another one with a 2-D sheet structure were obtained instead.

Single-Crystal X-ray Diffraction. A suitable dark green crystal with dimensions of 0.15 × 0.2 × 0.2 mm was selected for indexing and intensity data collection on a Siemens SMART CCD diffractometer equipped with a normal focus, 3 kW sealed tube X-ray source. Intensity data were collected at room temperature in 1271 frames with ω scans (width 0.30° per frame). Empirical absorption corrections based on symmetry equivalents were applied ($T_{min,max}$ = 0.816, 0.952).[22] Of the 9652 reflections collected ($2\theta_{max}$ = 56.6°), 2594 unique reflections were considered observed [$I > 2\sigma(I)$] after data reduction. The structure was solved by direct methods: the V and P atoms were first located and the O, C, and N atoms in the framework were found in difference Fourier maps. Bond-valence calculation results indicate that O(6) is a hydroxo oxygen atom,[23] and there are two PO_4^{3-} groups and one $H_2PO_4^-$ group per formula unit. The H atom bonded to O(6) was also found. Two atom sites were located in the structural window, which can be ascribed to lattice water oxygen and ammonium nitrogen atom. Both sites are half occupied, and the very short distance between them indicates that the two molecules are not simultaneously present in the same structural window within a unit cell. On the basis of elemental analysis and magnetic susceptibility (vide infra), the site at the general position is assigned to nitrogen and the one on the 2-fold axis to the oxygen atom. The ammonium and water hydrogen atoms were not located. The hydrogen atoms, which are bonded to carbon atoms, were positioned geometrically and refined using a riding model with fixed isotropic thermal parameters. The final cycles of least-squares refinement included atomic coordinates and anisotropic thermal parameters for all non-hydrogen atoms. The final difference Fourier maps were flat ($\Delta\rho_{max,min}$ = 0.48, −0.37 e/Å^3). All calculations were performed using the SHELXTL Version 5.1 software package.[24]

Magnetic Susceptibility Measurements. Variable-temperature magnetic susceptibility $\chi(T)$ data were obtained on 106.1 mg of a polycrystalline sample of **1** from 5 to 300 K in a magnetic field of 5 kG after zero-field cooling using a SQUID magnetometer. Correction for diamagnetism was made according to Selwood.[25]

Solid State NMR Measurements. All NMR spectra were acquired on a Bruker AVANCE−400 spectrometer, operating at 400.13 and 161.73 MHz for ^{1}H and ^{31}P, respectively. A Bruker probe equipped with 4 mm rotors for MAS (magic angle spinning) allowed spinning speeds of up to 15 kHz to be achieved. Typically, ^{1}H MAS NMR spectra were acquired with $\pi/2$ pulse widths of 4.0 μs, repetition times of 4 s, and spectrum widths of 100 kHz. Pulse lengths of 2.5 μs (45° flip angle) and recycle delays of 40 s were found to be adequate for quantitatively reliable ^{31}P MAS NMR spectra under conditions of high-power proton decoupling. The Hartmann−Hahn condition for ^{1}H → ^{31}P CP (cross-polarization) was determined by using $(NH_4)H_2PO_4$. Chemical shifts of ^{1}H and ^{31}P were externally referenced to tetramethylsilane (TMS) and 85% H_3PO_4, respectively. ^{1}H → ^{31}P CP/MAS spectra were recorded as a function of the contact time ranging from 0.1 to 30 ms.

Results and Discussion

Description of the Structure. The crystallographic data and selected bond lengths for **1** are given in Tables 1 and 2, respectively. It crystallizes in the monoclinic space group $C2/c$ with a unit cell content of four formula units. P(2) and the lattice water oxygen atom have a local symmetry of C_2, and all other atoms are at general positions. There are two unique vanadium atoms in an asymmetric unit. On the basis of charge-balance considerations **1** is a mixed-valence vanadium(IV,V) compound.

The structure consists of dimers of edge-sharing octahedra that are connected by corner-sharing phosphate tetrahedra to form layers in the *ab*-plane, which are further linked

(19) Chen, C.-Y.; Lo, F.-R.; Kao, H.-M.; Lii, K.-H. *Chem. Commun.* **2000**, 1061.
(20) Jiang, Y.-C.; Lai, Y.-C.; Wang, S.-L.; Lii, K.-H. *Inorg. Chem.* **2001**, *40*, 5320.
(21) Huang, L.-H.; Kao, H.-M.; Lii, K.-H. *Inorg. Chem.* **2002**, *41*, 2936.
(22) Sheldrick, G. M. *SADABS*; Siemens Analytical X-ray Instrument Division: Madison, WI, 1995.
(23) Brown, I. D.; Altermatt, D. *Acta Crystallogr.* **1985**, *B41*, 244.
(24) Sheldrick, G. M. *SHELXTL Programs*, version 5.1; Bruker AXS GmbH: Karlsruhe, Germany, 1998.
(25) Selwood, P. W. *Magnetochemistry*; Interscience: New York, 1956.

Table 1. Crystallographic Data for $NH_4[(V_2O_3)_2(4,4'\text{-bpy})_2(H_2PO_4)(PO_4)_2]\cdot 0.5H_2O$

empirical formula	$C_{20}H_{23}N_5O_{18.5}P_3V_4$
fw	926.105
space group	*C*2/*c* (No. 15)
a, Å	12.6354(8)
b, Å	9.9786(6)
c, Å	23.369(1)
β, deg	92.713(1)
V, Å^3	2943.1(3)
Z	4
T, °C	23
λ(Mo Kα), Å	0.71073
ρ_{calc}, g·cm^{-3}	2.090
μ(Mo Kα), cm^{-1}	14.9
R_1[a]	0.0389
wR_2[b]	0.1040

[a] $R_1 = \sum||F_o| - |F_c||/\sum|F_o|$. [b] $wR_2 = \{\sum[w(F_o^2 - F_c^2)^2]/\sum[w(F_o^2)^2]\}^{1/2}$, $w = 1/[\sigma^2(F_o^2) + (aP)^2 + bP]$, $P = [\text{Max}(F_o,0) + 2(F_c)^2]/3$, where $a = 0.0474$ and $b = 6.44$.

Table 2. Bond Lengths (Å) for $NH_4[(V_2O_3)_2(4,4'\text{-bpy})_2(H_2PO_4)(PO_4)_2]\cdot 0.5H_2O$[a]

V(1)−O(1)	2.017(2)	V(1)−O(3)	1.952(2)
V(1)−O(5)	2.380(2)	V(1)−O(7)	1.597(2)
V(1)−O(8)	1.752(2)	V(1)−N(1)	2.171(3)
V(2)−O(2)	1.958(2)	V(2)−O(4)	1.992(2)
V(2)−O(5)	2.290(2)	V(2)−O(8)	1.951(2)
V(2)−O(9)	1.593(3)	V(2)−N(2)	2.164(3)
P(1)−O(1)	1.547(2)	P(1)−O(2)	1.516(2)
P(1)−O(3)	1.546(2)	P(1)−O(4)	1.535(2)
P(2)−O(5)	1.507(2) (2×)	P(2)−O(6)	1.562(3) (2×)
N(1)−C(1)	1.319(5)	N(1)−C(5)	1.306(5)
C(1)−C(2)	1.377(6)	C(2)−C(3)	1.372(6)
C(3)−C(4)	1.364(5)	C(3)−C(8)	1.483(5)
C(4)−C(5)	1.377(6)	N(2)−C(6)	1.340(5)
N(2)−C(10)	1.335(4)	C(6)−C(7)	1.390(5)
C(7)−C(8)	1.393(5)	C(8)−C(9)	1.386(5)
C(9)−C(10)	1.372(5)	O(6)−H(6O)	0.893

[a] The C−H bond lengths are 0.93 Å.

through 4,4′-bpy pillars to generate a 3-D framework (Figure 1). The 4,4′-bpy ligand is nearly planar with the two pyridyl rings twisted by 7.3°. Within a layer there are 10-sided windows formed by the edges of five octahedra and five tetrahedra (Figure 2). The ammonium cations and lattice water molecules are located in the windows within each layer and form hydrogen bonds with framework oxygen atoms, as inferred from the Ow···O and N(3)···O distances.

Each vanadium atom is bonded to one N and five O atoms to form a distorted octahedron (Figure 3). Both V(1) and V(2) form a vanadyl group (V═O) with a terminal oxygen atom being strongly bonded [V(1)−O(7) = 1.597 Å and V(2)−O(9) = 1.593 Å]. The second shortest V−O bonds are toward the bridging oxygen O(8), with V(1)−O(8) = 1.752 Å, V(2)−O(8) = 1.951 Å, and ∠V(1)−O(8)−V(2) = 121.5°. The longest bonds are those to O(5) from a H_2PO_4 group *trans* to the vanadyl oxygen atoms. The second longest bonds are those to the nitrogen atoms from 4,4′-bpy. The mean V−(O,N) bond lengths of the two octahedra are 1.978 Å for V(1) and 1.991 Å for V(2), which is indicative of a higher oxidation state for V(1). To our knowledge a mixed-valence vanadium(IV,V) edge-sharing bioctahedron has not been reported before. Several vanadium(V) phosphates which consist of dimers of edge-sharing octahedra were reported. For example, each V^VO_6 octahedron in $Ag_2VO_2PO_4$ contains

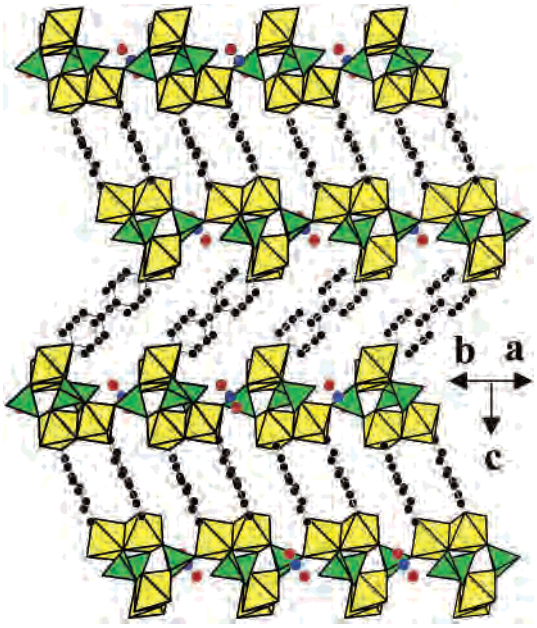

Figure 1. Structure of $NH_4[(V_2O_3)_2(4,4'\text{-bpy})_2(H_2PO_4)(PO_4)_2]\cdot 0.5H_2O$ (**1**) viewed along the [110] direction. The VO_5N octahedra are shown in yellow, and phosphate tetrahedra in green. Black circles, C atoms; blue circles, water O atoms; red circles, ammonium N atoms.

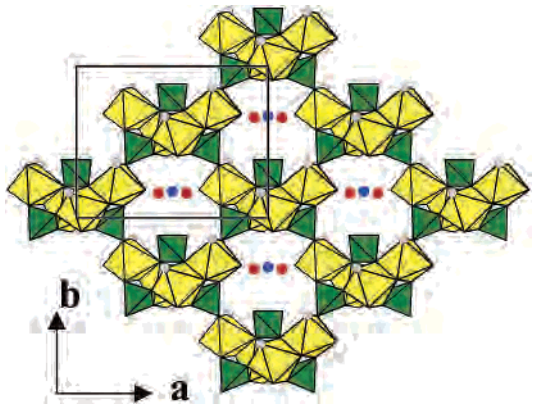

Figure 2. Section of a VPO layer in **1** viewed along the *c*-axis. The VO_5N octahedra are shown in yellow, and phosphate tetrahedra in green. Gray circles, 4,4′-bpy N atoms; blue circles, water O atoms; red circles, ammonium N atoms.

two short (1.620, 1.689 Å), two medium (1.958, 1.958 Å), and two long (2.139, 2.318 Å) V−O bond distances.[26] The oxidation states of V(1) and V(2) in **1** are indicated from a comparison of their V−O bond lengths with those in $Ag_2VO_2PO_4$ to be 5+ and 4+, respectively. There are two distinct phosphate groups in **1**. $P(1)O_4$ forms a bridge over two V atoms in a dimer and coordinates to two V atoms belonging to two different dimers. $H_2P(2)O_4$ shares its two oxygens with four octahedra belonging to two dimers with the two hydroxo groups being directed toward the center of the 10-sided window. It is worthy of note that the oxygen atoms from $P(1)O_4$ form shorter V−O bonds than those from H_2PO_4.

Magnetic Susceptibility. Plots of χ_M and $\chi_M T$ vs *T* for **1** are shown in Figure 4. The thermal evolution of χ_M follows

(26) Kang, H.-Y.; Wang, S.-L.; Tsai, P.-P.; Lii, K.-H. *J. Chem. Soc., Dalton Trans.* **1993**, 1525.

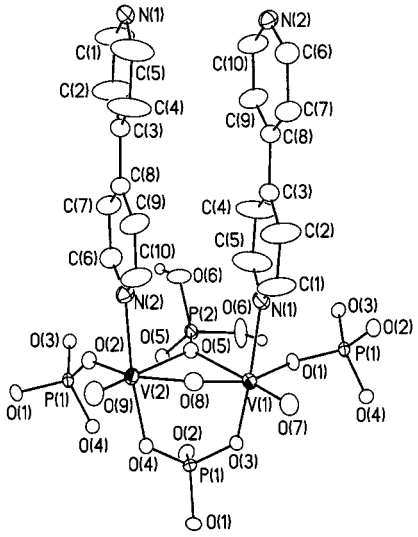

Figure 3. Local coordination of the vanadium atoms in **1** showing the atom-labeling scheme and ellipsoids at 50% probability. Small open circles represent hydrogen atoms.

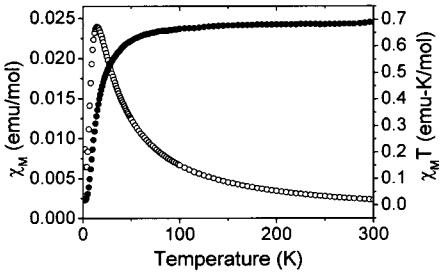

Figure 4. Thermal dependence of χ_M (open circles) and $\chi_M T$ (solid circles) for **1**.

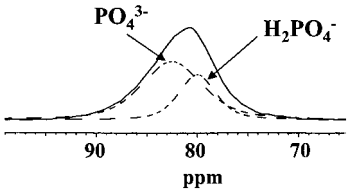

Figure 5. Proton-decoupled ^{31}P MAS NMR spectrum for **1** acquired at a spinning speed of 15 kHz. The dashed lines represent the components used to fit the spectrum.

the Curie−Weiss law at temperatures > 50 K, with $C_m = 0.699$ cm^3·K·mol^{-1} and $\theta = -9.1$ K, exhibiting a maximum in χ_M at 12 K. This result together with the decrease in the $\chi_M T$ values below 100 K are indicative of antiferromagnetic interaction in the compound. The effective magnetic moment per octahedral dimer ($\mu_{eff} = 2.83(0.699/2)^{1/2} = 1.67\ \mu_B$) compares well with the spin-only moment (1.73 μ_B) calculated for a mixed-valence vanadium(IV,V) dimer. Therefore, the valence of the vanadium atoms in **1** is confirmed by magnetic susceptibility.

^{31}P MAS NMR. Figure 5 is the proton-decoupled ^{31}P MAS NMR spectrum of **1**, obtained at a spinning speed of 15 kHz. The spectrum displays a broad resonance, which was fitted in accordance with the stoichiometry of **1** to two peaks in an intensity ratio close to 1:2, as shown as dashed lines in the figure. To assign the peaks, ^{1}H → ^{31}P CP/MAS NMR experiments with various contact times were performed. At short contact time (e.g., 150 μs), the resonance at 80 ppm, as compared with that at 83 ppm, shows a much faster magnetization transfer from proton spins. This indicates that the former resonance experiences a stronger ^{1}H−^{31}P dipolar coupling and thus is in closer proximity to hydrogen atoms. Therefore, the resonances at 80 and 83 ppm can be assigned to the $H_2P(2)O_4$ and $P(1)O_4$ site, respectively.

Variable-Temperature ^{31}P NMR Study. It has been reported that for diamagnetic metal phosphates the isotropic ^{31}P chemical shifts move to high-field values with decreasing protonation. For example, the chemical shifts of H_2PO_4, HPO_4, and PO_4 groups in a series of layered Ti, Zr, and Al phosphates appear around −10, −20, and −30 ppm, respectively.[27] For $[Ga_4(C_{10}H_9N_2)_2(PO_4)(H_{0.5}PO_4)_2(HPO_4)_2(H_2PO_4)_2(H_2O)_2]\cdot H_2O$, the four peaks at −0.4, −0.92, −11.3, and −17.9 ppm can be assigned to the four distinct P sites H_2PO_4, HPO_4, $H_{0.5}PO_4$, and PO_4, respectively.[19] The observed large downfield shifts for **1** can be ascribed to magnetic exchange coupling involving phosphorus atoms. The $P(1)O_4$ group has a larger downfield shift than that for $H_2P(2)O_4$, indicative of higher unpaired electron spin density at P(1). We explain that the PO_4 group is observed from a comparison of the V(2)−O bond lengths to form stronger bonds to $V(2)^{4+}$.

The experimental NMR signal shifts, δ^{exp}, of paramagnetic species are composed of a paramagnetic contribution, δ^{para}, and a diamagnetic contribution, δ^{dia}. Here we are interested in the effect of the unpaired electron at the V(2) site on the ^{31}P NMR shifts. In principle, there are two important interactions that govern the paramagnetic shifts caused by unpaired electrons. One involves the Fermi contact shift that arises from the isotropic interaction of the nuclear spin and the net electron spin density at the nucleus, and the other is pseudo-contact shift due to anisotropic dipolar interaction of the electron spin and the nuclear spin. The Fermi contact shift predominates owing to weak spinning sidebands in the ^{31}P MAS NMR spectra. The dipolar shift contributions to the paramagnetic shift, δ^{para}, are negligible because *g*-factor anisotropy is generally small.[28,29] The thermal variation of δ^{para} is given by eq 1.[28]

$$\delta^{para} = -A_N(\gamma_e/\gamma_N)hS(S+1)10^6/3kT \qquad (1)$$

where A_N is the Fermi contact hyperfine coupling constant, γ_e and γ_N are the gyromagnetic ratios of electron and nuclear spin, respectively, k is the Boltzmann constant, h is the Planck constant, and T is the absolute temperature. The sign of A_N determines the sign of the spin density transferred to the resonant atom and thus the direction of the shift. Figure 6a shows the variable-temperature ^{31}P MAS NMR spectra. The observed frequency shift decreases with increasing temperature from 100 ppm at 213 K to about 78 ppm at 313 K. The line width also slightly decreases with temperature. The linear variation of the frequency shift versus $1/T$ is shown in Figure 6b. The intercept δ^{dia} is 32.7 ppm, and the

(27) Nakayama, H.; Eguchi, T.; Nakamura, N.; Yamaguchi, S.; Danjyo, M.; Tsuhako, M. *J. Mater. Chem.* **1997**, *7*, 1063.
(28) Drago, R. S. *Physical Methods for Chemists*; Saunders College Publishing: Ft. Worth, TX, 1992; Chapter 12.
(29) D'Anna, J. A.; Wharton, J. H. *J. Chem. Phys.* **1970**, *53*, 4047.

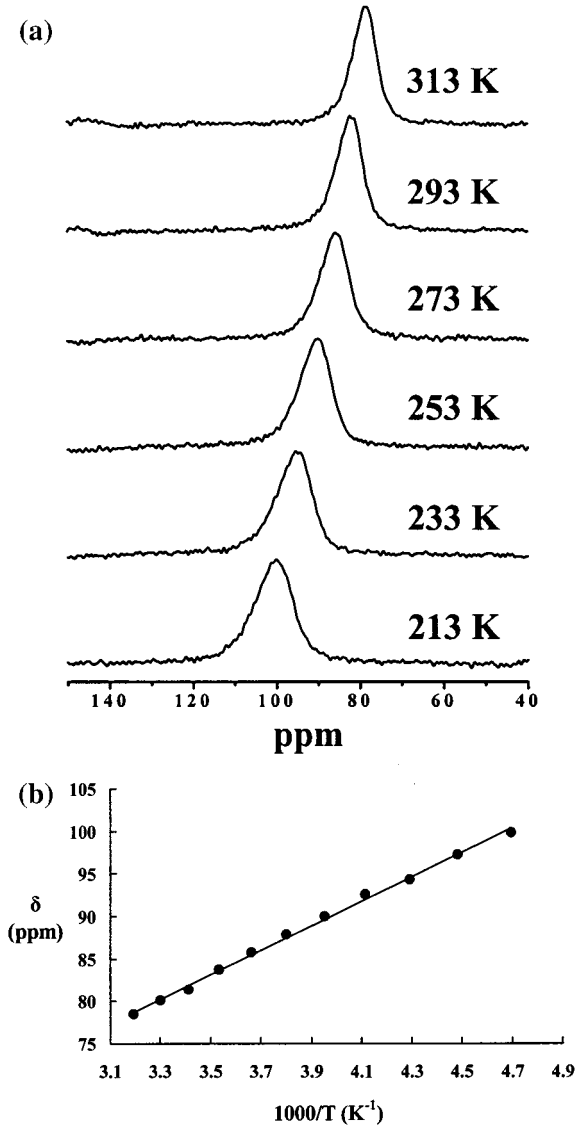

Figure 6. (a) Variable-temperature ^{31}P MAS NMR spectra for **1** (spinning speed = 10 kHz). (b) Temperature dependence of ^{31}P chemical shifts. The solid line represents the linear curve fit to the experimental data.

paramagnetic shift $\delta^{para} = \delta^{exp} - \delta^{dia}$ is ca. 50 ppm at room temperature. A_N can now be easily calculated from the paramagnetic shift δ^{para} (in ppm) according to the relation $A_N = 0.141\delta^{para}\gamma_N \times 10^{-3}$, which follows from eq 1 with $T = 300$ K and $S = 1/2$. A value of 760 kHz is obtained for A_N. Moreover, the relation between A_N and the unpaired electron spin density at the interacting nucleus is given by eq 2.

$$A_N = (8\pi/3)g_e\mu_B\gamma_N\rho_n \qquad (2)$$

where g_e is the electron g-factor, μ_B is the Bohr magneton, and ρ_n is the unpaired electron spin density at the resonant nucleus. Thus, ρ_n can also be determined from the NMR spectra and amounts to an average value of about 4.7×10^{-4} au.

^{1}H MAS NMR. Figure 7 shows the variable-temperature ^{1}H MAS NMR spectra of **1**, acquired at a spinning speed of 10 kHz. A major resonance at 8.4 ppm with two shoulders

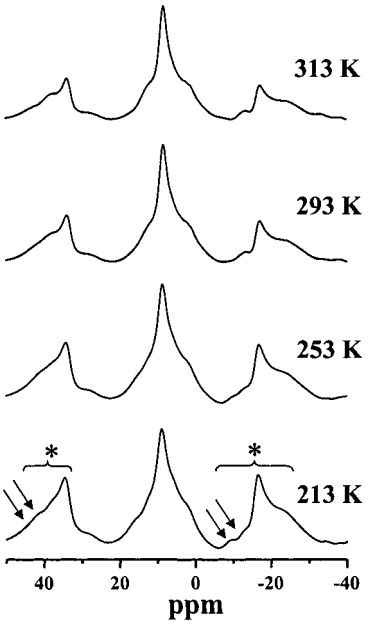

Figure 7. Variable-temperature ^{1}H MAS NMR spectrum of **1** (spinning speed = 10 kHz). Two sets of spinning sidebands become resolvable at low temperatures as indicated by arrows.

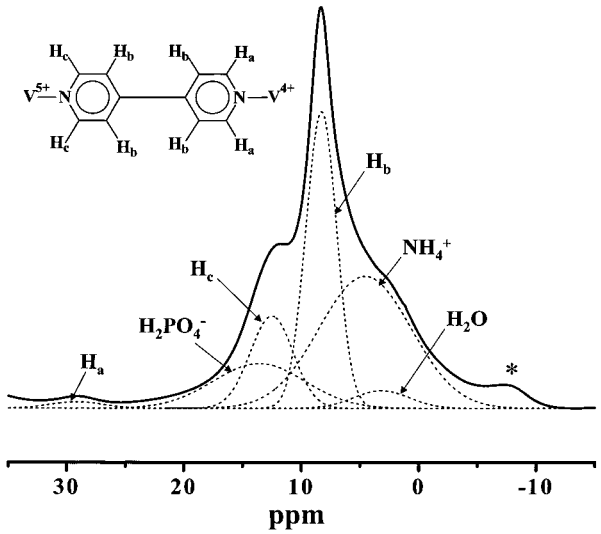

Figure 8. Room-temperature ^{1}H MAS NMR spectrum of **1**, acquired at a spinning speed of 15 kHz, fitted with six components for different types of protons.

at ca. 13 and 5 ppm was observed. The spectrum at 213 K reveals two sets of sidebands associated with the shoulder at ca. 13 ppm, indicating that the shoulder consists of two overlapping signals. The peak at 29.2 ppm with a much lower shift is an isotropic resonance instead of a spinning sideband, as indicated from a spectrum taken at a higher spinning speed (e.g., 15 kHz). It can be assigned to the H_a protons in the pyridyl ring because these protons are in closer proximity to $V(2)^{4+}$. The resonance in the range from 12 to 20 ppm was fitted to two peaks because of the appearance of two sets of sidebands at low temperature. Compared with the ^{1}H NMR spectrum of $(NH_4)H_2PO_4$, the peaks at 13.6 and 4.6 ppm are assigned to $H_2PO_4^-$ and NH_4^+, respectively. Their broad line widths can be ascribed to hydrogen bonds. The resonances at 12.6 and 8.4 ppm are assigned to the H_c and

H_b, respectively. The ^1H NMR spectrum was fitted to six components, as shown in dashed lines in Figure 8. The intensity ratio of the six resonances at 29.2, 13.6, 12.6, 8.4, 4.6, and 3.2 ppm including the intensities of spinning sidebands is close to the stoichiometry of **1** (4:2:4:8:4:1) as determined from X-ray diffraction.

In summary, the hydrothermal synthesis of a new vanadium phosphate and its crystal structure have been described in this work. The structure consists of layers of mixed-valence vanadium(IV,V) phosphate pillared through 4,4′-bpy ligands into a 3-D structure. It is the first mixed-valence compound in the 4,4′-bpy-phosphate system. Magnetic susceptibility confirms the valence of the vanadium atoms. Variable-temperature ^{31}P MAS NMR experiments have been performed to determine the unpaired electron spin density at the phosphorus nucleus. The results obtained from spectral decomposition of the observed ^1H MAS NMR spectrum confirm the structure and stoichiometry as determined from X-ray diffaction. We aim to combine the flexibility of metal organic coordination systems with the thermal stability of the phosphate materials to produce new open frameworks. Further research on this theme is in progress.

Acknowledgment. We thank the National Science Council for support and Ms. R.-R. Wu at the National Cheng Kung University for NMR measurements.

Supporting Information Available: X-ray crystallographic files in CIF format for the structure determination of **1**. This material is available free of charge via the Internet at http://pubs.acs.org.

IC011277I